

Growth of Epitaxial Zinc Oxide Thin Films onto Gallium Nitride by Electrodeposition from a Dimethylsulfoxide Based Electrolytic Solution

Humberto Gómez^{1,*}, Solange Cantillana¹, Gonzalo Riveros², Sofia Favre³, Carlos J. Pereyra³, Daniel Ariosa³, Ricardo E. Marotti³, Enrique A. Dalchiele³

¹Instituto de Química, Facultad de Ciencias, Pontificia Universidad Católica de Valparaíso, Casilla 4059, Valparaíso, Chile.

²Departamento de Química y Bioquímica, Facultad de Ciencias, Universidad de Valparaíso, Avenida Gran Bretaña 1111, Playa Ancha, Valparaíso, Chile.

³Instituto de Física & CINQUIFIMA, Facultad de Ingeniería, Herrera y Reissig 565, C.C. 30, 11000 Montevideo, Uruguay.

*E-mail: hgomez@ucv.cl

Received: 22 May 2013 / Accepted: 5 July 2013 / Published: 1 August 2013

Zinc oxide films have been electrochemically grown on gallium nitride substrates from an electrolytic bath composed of a zinc salt and oxygen dissolved in dimethylsulfoxide (DMSO). The XRD structural study showed the epitaxial growth of the films, specifically it was found that the *c* axis is perpendicular to the plane of the substrate, while *a* and *b* axes are aligned with the respective substrate lattice parameters. In spite the similarity of both crystal structures and the close values of their lattice parameters, for thinner films it was possible to detect a component under in-plane compression while thicker films presumably relax. The obtained Poisson's ratio for ZnO was in good agreement with tabulated values, indicating a real effect of elastic deformation and confirming the consistency of the performed analysis. The optical properties of the performed electrodeposited film showed that the transmittance spectra have a very similar general shape in comparison with the one of the substrate but with an increase in the total optical transmittance. Due to presence of ZnO, the diffused reflectance spectra showed also an increased absorption close to 400 nm. As a consequence of the difference in the defect density, the photoluminescence measurements recorded in stressed and relaxed samples also changes drastically.

Keywords: Zinc Oxide, Gallium nitride, epitaxial electrodeposition, DMSO, structural characterization, optical characterization.

1. INTRODUCTION

Zinc oxide is a large band gap (~ 3.3 eV) *n*-type semiconductor which is of interest for high-frequency piezoelectric resonators, conducting transparent windows for photovoltaic cells, and UV

light-emitting devices. The growth of epitaxial ZnO thin films has been studied for acoustical and optical devices because of their tendency to grow with strong [0001] preferential orientation on various kinds of substrates, including glass [1], sapphire [2], and diamond [3]. In order to reduce the strains and dislocation density in epitaxial ZnO and related films, closely lattice-matched are favored which is the case for the epitaxial growth of ZnO on GaN, because of the 1.9% lattice mismatch between both hexagonal compounds for the a parameter. Epitaxial ZnO films have been grown on both basal plane sapphire and silicon substrates with a variety of vapor deposition methods, including metal organic chemical vapor deposition [4, 5], pulsed laser deposition [6], molecular beam epitaxy [7] and radio-frequency magnetron sputtering [8]. More recently, it has been reported that epitaxial ZnO films can be synthesized on (111) spinel [9], and (0001) GaN buffered Al₂O₃ substrates [10] in water at 90 °C.

Electrochemical deposition in aqueous solution is a low temperature alternative route well adapted to prepare epitaxial ZnO films on n -GaN [11-14]. Besides, as reported by O. Lupan *et al.* [15], due to the electron exchange during the film growth, electrochemical deposition favors a good electric contact between both compounds, which is an additional advantage for the production of optoelectronic devices. In aqueous solution, the deposition of ZnO proceeds through an electrochemically induced interfacial precipitation through the generation of an intermediate soluble species (hydroxide ions) produced from the reduction of precursors such as oxygen, nitrate ions or hydrogen peroxide. The interest is that precipitation can be more easily controlled via the electrochemical potential. The possibility of epitaxial growth is a direct consequence of the high selectivity of the nucleation process of ZnO from solution and the fact that the growth takes place under quasi-equilibrium conditions. The dissolution/precipitation processes involved tend to minimize the energy of the system, which allows the optimization of epitaxial relations and the formation of high quality materials [16].

Electrochemical deposition of ZnO can also be achieved in non-aqueous solvents, such as dimethylsulfoxide (DMSO) [17]. The interest in using DMSO stems from the possibility to increase the electrodeposition bath temperature because of its boiling point (189° C), higher than the one of water and a wide operating potential range and consequently the absence of ubiquitous hydrogen evolution reaction. The reaction mechanism involved in the electrochemical formation of a ZnO film in a DMSO solution is not based on hydroxide ions, and, for oxygen as precursor, may correspond to a different recently reported mechanism [18, 19]. Moreover, the crystal surface properties, which are of particular importance for properties such as luminescence, are likely to be different for both aqueous and non-aqueous electrolytic baths. In the current paper, we report the epitaxial growth of ZnO on GaN which was clearly evidenced by texture X-ray diffraction analysis. The as grown deposits presented high structural and optical quality, without any further thermal annealing, opening thus the possibility for the heteroepitaxial structure to be integrated in optoelectronic devices.

2. EXPERIMENTAL PART

2.1 ZnO electrodeposition

Previous to the electrodeposition, GaN wafers (Kyma Technologies, USA) were cut with a diamond knife and cleaned according to the procedure used in reference [15]: The samples were

degreased in hot acetone (53° C) for 12 minutes followed by 12 minutes in methanol at room temperature, both in an ultrasonic cleaner. The samples were rinsed with deionized water (resistivity 18.2 mΩ cm), and then subsequently treated with hot concentrated NH₃ (28%, 60° C) for 10 minutes, with HCl:H₂O 1:1 for 12 minutes and, finally rinsed with deionized water. Once cleaned, the GaN samples were immediately utilized to avoid surface oxide formation. To be used as working electrodes, the GaN samples were put on a copper holder, and the electric contacts were made with a drop of eutectic Ga/In.

All the electrochemical experiences were performed in a conventional electrochemical cell with three electrodes: Reference electrode (saturated Ag/AgCl electrode), counter electrode (Pt); and working electrode (GaN). This cell was maintained in a glycerin bath with a hot plate to control the operation temperature (80° C). The electrolytic solution was a 50 mM ZnCl₂ dissolved in dry DMSO without any supporting electrolyte. Previous to the electrodeposition, the electrolytic solution was bubbled with molecular oxygen for 10 minutes to obtain an O₂ saturated solution. During the electrodeposition, the solution was maintained within an oxygen atmosphere and without mechanic stir. The electrodeposition was carried out at constant potential between -1.4 V and -1.6 V at different times to obtain different thickness.

2.2. Morphological and Structural Characterization

Atomic force microscopy (AFM) was employed to characterize the surface of GaN substrate and ZnO thin film morphology. The measurements were performed in tapping mode in air using multimode scanning probe microscope Nanoscope IIIa equipment (Digital Instrument, Santa Barbara, CA).

The structural characterization was carried through X-ray diffraction (XRD) measurements. Standard $\theta - 2\theta$ scans were performed on a Philips PW180 diffractometer (30kV, 40mA, CuK α radiation with $\lambda = 1.5406\text{\AA}$). The diffraction peaks from ZnO and GaN have been indexed by reference to the JCPDS powder diffraction files. Rocking-curves (RC) and Pole figures were obtained, with the same radiation source, on a Philips X'Pert MRD goniometer.

In order to check the presence of only 00l reflections, standard $\theta - 2\theta$ XRD scans were performed in Bragg-Brentano geometry over a wide range of angles. We focused on the study of the (004) Bragg reflection, from both contributions: film and substrate. To detect the weak contributions from the film, we had to increase the signal/noise ratios, using longer acquisition times for the diffraction pattern.

2.3 Optical Characterization

The samples were optically characterized by transmittance, diffuse reflectance and photoluminescence (PL). For transmittance the experimental setup consisted in a 1000 W electric power Xe lamp (ORIEL 6271), whose output reaches the sample after being chopped (by an SRS SR540 chopper) and monochromated (by an ORIEL 77250 monochromator). The transmitted light was

detected with an UDT 11-09-001-1 (100 mm² wide area UV enhanced unbiased silicon detector). A first lock-in amplifier (SRS SR530) extracted the signal from the detector. A second one (EG&G 5209) was used for noise reduction, measuring the amplitude variation of the light source, and correcting the fluctuations in the first lock-in through the ratio output. For diffuse reflectance, the reflected light (normal detection and quasnormal incidence [20]) were measured. In this case a SR570 current preamplifier was added due to the very low diffused light reflected by these almost transparent samples. In both, transmittance and reflectance measurement, the lamp spectrum was used as reference because of the interference fringes present in the bare substrate. Moreover, the proximity of the absorption edge of ZnO with the one of the GaN substrate complicate the measurements, as will be shown on the Results and Discussion section.

The PL spectra were measured using a calibrated S2000 Ocean Optics spectrometer, and exciting with a 300nm UVTOP295-BL-TO39 LED obtained from ROITHNER LASERTECHNIK GmbH. A band-pass U-340 optical filter (from UQG Optics) was used before the sample to filter visible light emitted by the LED and a long-pass GG-395 optical filter (also from UQG Optics) was used after the sample to filter UV light from the LED. All optical measurements were done at room temperature.

3. RESULTS AND DISCUSSION.

3.1. Electrodeposition of ZnO thin films

Figure 1 shows the voltammetric response of a n-type GaN electrode in a 0.05 M ZnCl₂ DMSO solution, in the absence and in the presence of dissolved molecular oxygen. In the first case, the observed cathodic current from -1.3 V towards negative potentials is attributed to the Zn(II) reduction to metallic zinc.

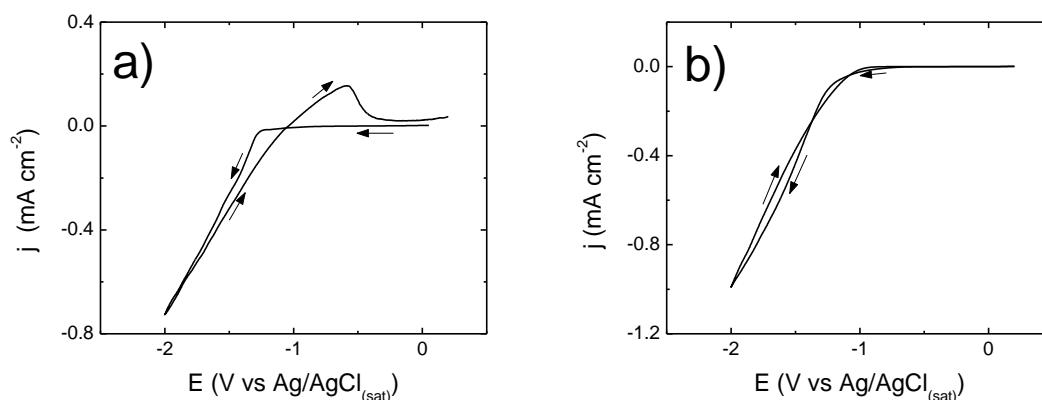


Figure 1. Voltammetric response of a n-type GaN electrode in a 0.05 M ZnCl₂ DMSO electrolytic bath solution at 80° C a) in the absence and b) in the presence of dissolved molecular oxygen. Scan rate: 20 mV s⁻¹.

The anodic current corresponds to the re-oxidation of the metallic zinc previously deposited. In the presence of dissolved molecular oxygen, only a cathodic process corresponding to the oxygen

reduction on the GaN surface is observed. Oxygen species produced in this process react with zinc ions to form ZnO through a heterogeneous precipitation reaction [18, 19].

According to these results, ZnO electrodeposition can be carried out at potentials more cathodic than -1.2 V. In our experiences, the films were potentiostatically deposited at -1.4 V and -1.6 V and at different times. Depending on the electrodeposition time (charge consumed during the ZnO electroformation) and the area of GaN exposed to the electrolytic bath solution, film thicknesses of ca. $0.1\ \mu\text{m}$ (sample 1), $0.2\ \mu\text{m}$ (sample 2) and $0.3\ \mu\text{m}$ (sample 3) were estimated.

3.2 Morphological characterization

Figure 2 shows the AFM images of the GaN substrate before and after ZnO electrodeposition. Previous to the electrodeposition, the substrate morphology is smooth and some steps and terraces can be observed along the surface. The height of the terraces is of 10 nm in average which is a common morphology in these kinds of films [20].

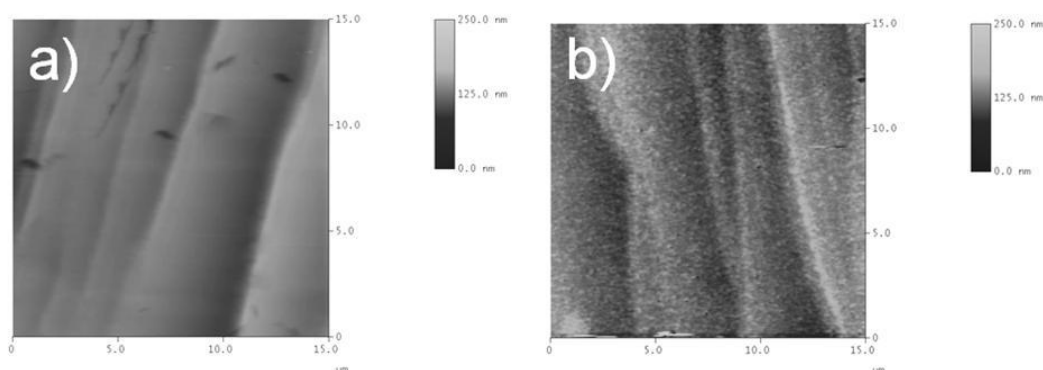


Figure 2. a) AFM image of GaN substrate previous to the ZnO electrodeposition. b) AFM of GaN substrate with a ZnO layer electrodeposited at -1.4 V and 80°C .

The morphology of the latter doesn't change when a thin layer of ZnO is deposited on the GaN, confirming that the ZnO films uniformly cover the substrate surface. The images show that the film is composed by small crystallites, a morphology that completely differs from the characteristic columnar growth of ZnO in aqueous solution [21].

3.3 Structural Characterization by XRD

Figure 3 shows a comparison between Pole figure for ZnO (film) and GaN (substrate). The figure shows a perfect alignment of the epitaxial film on the substrate. Standard $\theta-2\theta$ XRD scans in Bragg-Brentano geometry with high resolution around the (004) Bragg reflections were performed for each sample.

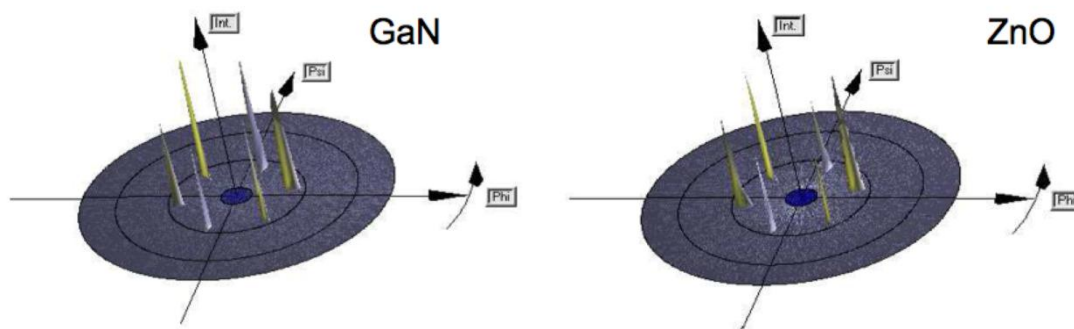


Figure 3. Pole figures for GaN (103) in (a) and ZnO (103) in (b).

In Figure 4, the results for the thinner and thicker samples are showed. The measurements were numerically filtered to remove the Cu-K α_2 contribution of the K α_1 -K α_2 doublet.

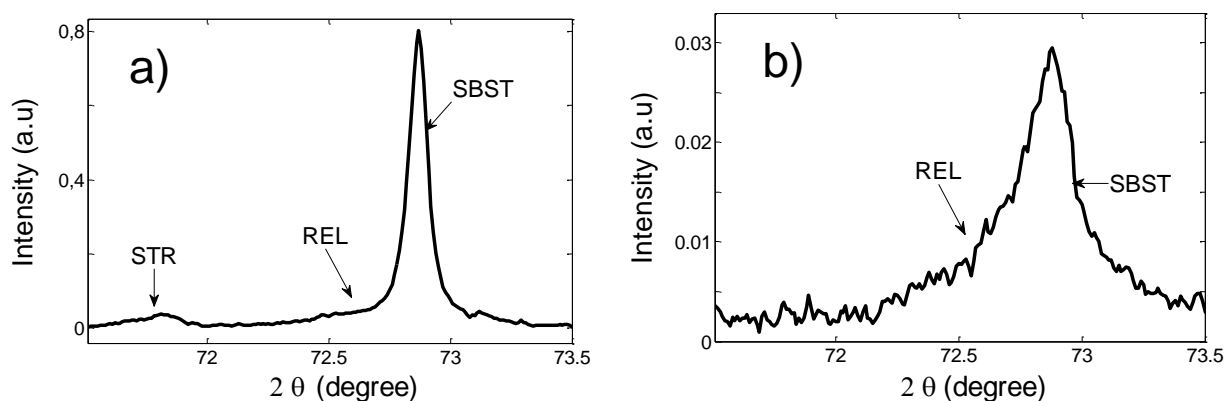


Figure 4. Bragg Brentano XRD spectra of an electrochemically grown ZnO thin film onto a GaN film, around 004 Bragg Reflection, for Sample 1 in (a) and Sample 3 in (b). Arrows indicate peak positions for GaN (SBST.), relaxed ZnO (REL.) and strained ZnO (STR.).

Table 1. Parameters extracted from the fits of the (004) Bragg reflection: 2θ - peak position ; Δ - peak width ; d - film thickness ; c – lattice constant.

Samples		2θ (degrees)	Δ (degrees)	d (Å)	c (Å)
1	Substrate	72.87	0.0863	—	5.188
	Relaxed Film	72.6	0.7050	159	5.205
	Film under tension	71.799	0.2424	630	5.255
3	Substrate	72.87	0.2655	—	5.188
	Relaxed Film	72.6	0.3113	2152	5.205

All the samples show the (004) reflection for the substrate at the expected position ($2\theta = 72.9$), and a weak component from the relaxed film ($2\theta = 72.6$). In order to separate substrate and film contributions, the spectra were fitted with two Lorentzians, in the vicinity of the substrate peak. The

results are presented in Table 1. From the widths of the curves the relaxed film thickness has been estimated.

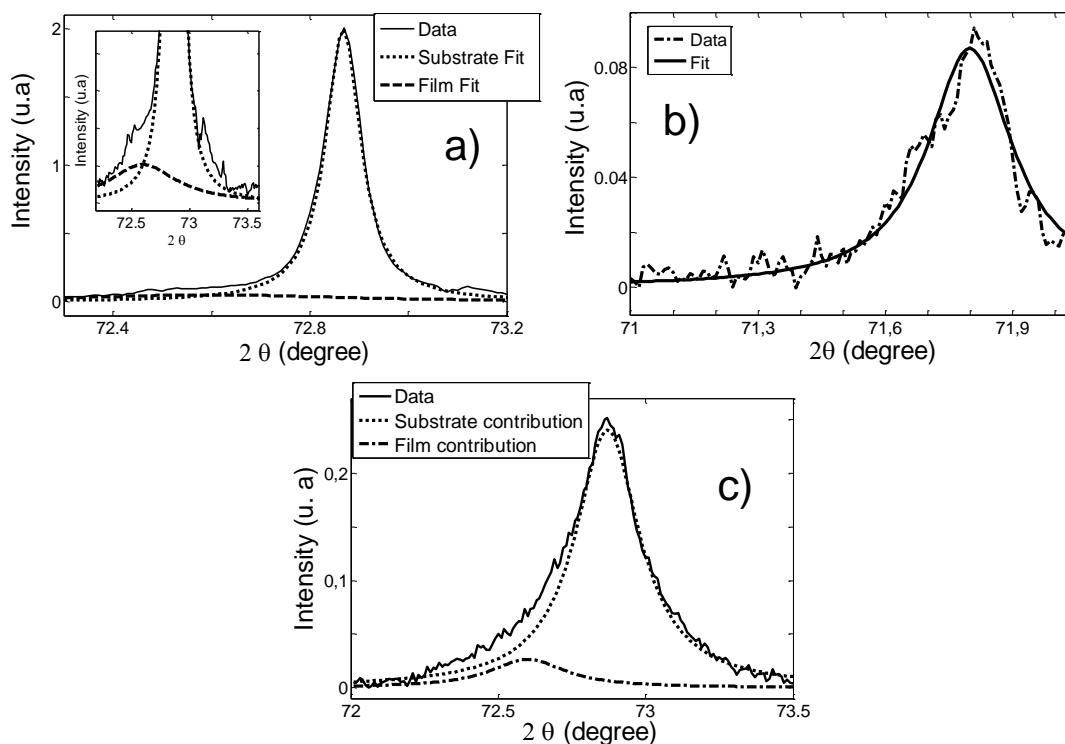


Figure 5. Bragg Brentano XRD spectra of ZnO – GaN, with Lorentzian fits around 004 Bragg reflection, for Sample 1 relaxed in (a), strained in (b), and Sample 3 in (c).

For the thinnest sample (sample 1), we found a clear contribution from the film under epitaxial strain at $2\theta = 71.8$, indicating an elongation of the c axis, from which one can guess that this part of the film is under in-plane compressive stress. This contribution was also fitted by a Lorentzian in order to extract the position and the width of the peak, from which the thickness of the strained layer was estimated. Figure 5, shows the detailed fits. In Table 1, films thicknesses are consistent with those determined from the growing parameters. A c -axis elongation of 0.96% is observed for the strained ZnO layer (630 Å thick) in sample 1.

Epitaxial stress is generally relaxed via misfit-dislocations, which reduces the film crystal coherence to a region of finite size ξ , the mean correlation length. Besides, the RC is the Fourier transform of the in-plane two-point correlation function. Thus, from its FWHM ($\Delta\Omega$), we can estimate the mean lattice correlation length (ξ) as follows:

$$\xi = c / (n\pi\Delta\Omega) \tag{1}$$

In equation (1), n is the index of the Bragg reflection, and c the lattice parameter.

Figure 6 illustrates the Rocking Curve (RC) performed around the strained ZnO (004) peak in sample 1.

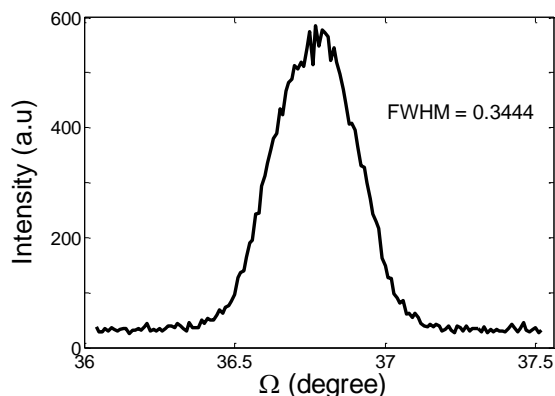


Figure 6 RC for the strained (004) layer in sample 1. The diffraction angle was fixed at the position $2\theta = 71.8^\circ$.

Assuming, now, that dislocations are only due to the difference between the in-plane lattice parameters of substrate and film, a measure of the correlation length ξ allow us to measure the in-plane strain $\epsilon_{//}$. Indeed, the crystal coherence of the strained epitaxial film along a given in-plane direction is conserved until it misses a unit cell of the substrate, leading to the formation of a dislocation. Then, the lattice parameter of the film obeys:

$$\xi = (m + 1)a_s = ma_F = ma_{0F}(1 + \epsilon_{//}) \tag{2}$$

Where m is the number of ZnO unit cells between consecutive dislocations, a_s the substrate lattice parameter, a_F the strained film lattice parameter, and a_{0F} the one for the relaxed film. Equation (2) yields:

$$\epsilon_{//} + 1 = \frac{\xi}{\xi - a_s} \frac{a_s}{a_{0F}} \tag{3}$$

Then, knowing the values a_s , a_{0F} and ξ , we can estimate the in-plane strain.

In the framework of the linear theory of elasticity, if we consider an uniaxial deformation where there is no applied tension along the direction perpendicular to the plane, and the in-plane deformations are isotropic ($\epsilon_x = \epsilon_y = \epsilon_{//}$), the Poisson's ratio ν obeys:

$$\frac{\epsilon_{\perp}}{\epsilon_{//}} = \frac{-2\nu}{(1 - \nu)} \tag{4}$$

From the FWHM of the RC we estimated a correlation length of 225Å, leading to an in-plane strain of -0.74% . Using the perpendicular strain calculated from the c-axis change, we obtained a Poisson's ratio of 0.39, in good agreement with tabulates values.

3.4 Optical Characterization

The optical properties of ZnO films grown onto GaN are not usually studied [11, 14] as both materials have very similar optical properties complicating the interpretation of the results. Figure 7 shows the results of the optical transmittance T spectrum of the substrate compared with those of the ZnO/GaN samples 1 and 3.

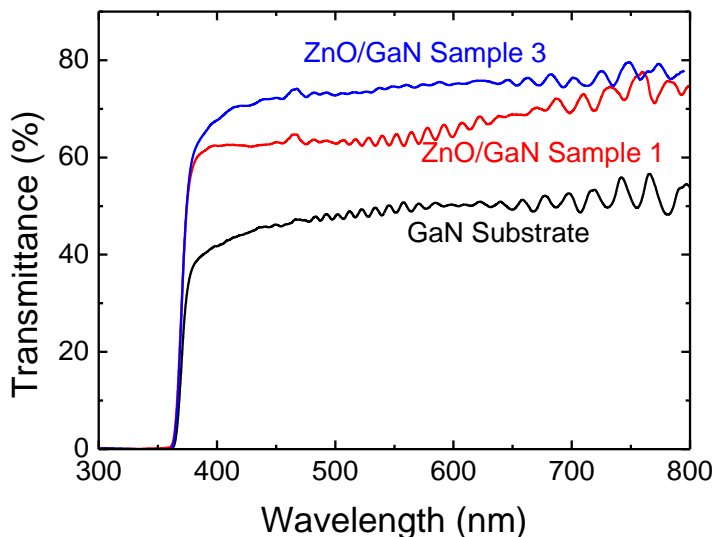


Figure 7. Optical transmittance spectra of samples 1 (red line) and 3 (blue line) compared with that of the substrate (black line).

For the substrate the main features are the absorption edge at the UV region and interference fringes. The absorption edge corresponds with a bandgap energy (obtained by usual $(-\ln T \times hv)^2$ against photon energy hv) at ~ 3.37 eV. This value is close to the well accepted value for GaN (3.4 eV) at room temperature [22]. However, the most accepted bandgap energy value for ZnO is also 3.37 eV [24-27], although there is a spread of reports between 3.1 to 3.4 eV [27-29]. For this reason the spectra of ZnO/GaN samples 1 & 3 in Figure 7 have an absorption edge at almost the same position. However the spectra for samples 1 & 3 change in comparison with the one of the substrate, mainly because the mean transmittance in the visible increases and the interference fringes change their position. Indeed, the visible transmittance for sample 3 is larger than 75 % while that of the substrate is close to 50 %. This can be understood as a consequence of the ZnO deposition because its refraction index is 2.0 [22, 29], which is an intermediate value between that of GaN (2.4) [22] and air. Therefore an index of refraction matching effect is generated and the ZnO acts as an antireflective coating, increasing light transmission through the sample. This antireflective effect is more effective for the thicker film (sample 3). On the other side, the interference fringes are less important for sample 3 which is the thicker one (see Table 1). For sample 1 two oscillations seem to be present: one similar to the one at the substrate and a smoother one probably originated in the very thin ZnO film.

Moreover, comparing the very small sample thicknesses of Table 1 with light penetration depth for ZnO, which is $\sim 1 \mu\text{m}$ at 360 nm [30] a very small influence of ZnO absorption edge is expected in transmittance measurements. This is in agreement with the almost unchanged position of the absorption edge in all spectra in Figure 7, as light transmitted through the sample is more influenced by GaN properties than those of ZnO. For that reason, diffused reflectance was measured and the results are shown in Figure 8. These measurements (diffused light in backscattering configuration) are more sensitive than transmittance measurements to very thin films absorption, as diffused light is mainly originated in the nearest face of the sample (Zn/GaN and ZnO/air interfaces). Indeed, in this configuration light interaction with the ZnO film would be stronger [31, 32].

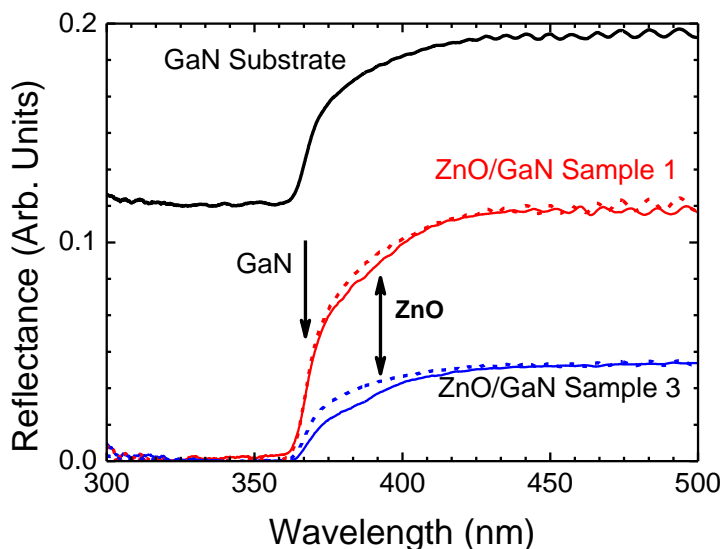


Figure 8. Diffuse Reflectance spectra of samples 1 (red line) and 3 (blue line) compared with that of the substrate (black line). Substrate spectrum (in full line) is vertically shifted, and dashed lines are the same spectra numerically adjusted to match same vertical span as samples 1 and 3. Vertical arrows indicate main features attributed to GaN and ZnO respectively.

The substrate spectrum in Figure 8 has the same general behavior than its corresponding transmittance spectrum in Figure 7: it consists in an absorption edge and interference fringes. This confirms that diffuse reflectance is an indirect way of measuring transmitted light [30]. The spectra for samples 1 and 3 in Figure 8 have also the same general features: an edge in the UV and interference fringes in the visible region. Once again the interference fringes are less important for the thicker film (sample 3). The index of refraction matching effect is also present in these measurements. Although the spectra are in arbitrary units, the reflected light for sample 3 is lesser than for sample 1, according to the higher transmittance of sample 3 compared with the one of sample 1, as observed in Figure 7. Moreover, a careful comparison between these spectra (samples 1 and 3) and the one of the substrate (vertically adjusted to reach the same value in the visible region) reveals a change in the shape of the edge: there is a reduced reflectance in the region between 350 and 400 nm. As the general shape of diffused reflectance and transmittance spectra are similar, this can be interpreted as an increased absorption originated in the ZnO films. Moreover this absorption is higher in thicker sample 3. Therefore an estimation of absorption edge for ZnO may be tried from diffused reflectance assuming it and indirect measurement of transmittance. After properly extracting a background to correct for the zero absorption line [33, 34], a value for the absorption edge for ZnO is obtained at ~ 3.15 eV. This value, although in the region of usually reported ZnO bandgap energy (between 3.1 to 3.4 eV [28-30]) is ~ 0.2 eV below the most accepted one. This may be due to the fact that bandgap energies are usually underestimated when obtained from reflectance measurements [32]. In the present case the need of considering a reduced spectral region below the GaN absorption edge adds further uncertainty. However this diffused reflectance measurement allows revealing the influence of the ZnO film on the optical properties.

PL measurements were done for further studying these optical properties. In order to separate the ZnO PL spectra from the substrate one, taking in consideration that GaN may have several emission bands [35], a numerical subtraction procedure was implemented over the experimental PL signal (I_{EP}). The substrate PL was measured before the deposition of the ZnO layer, obtaining in this way a background PL signal (I_{BP}) which will be also present in the ZnO/GaN samples PL. However, due to geometrical reasons and the presence of the different thickness in the ZnO films, its intensity may vary. Therefore, to achieve the subtraction I_{BP} should be properly scaled. For that scaling the ratio $\gamma = I_{EP} / I_{BP}$ is studied, particularly in the regions where the ratio is almost constant (γ_c). These regions represent zones where the ZnO/GaN PL is practically only due to the substrate emission. The constant value γ_c represents the influence in I_{EP} of the substrate. Then performing a γ_c -weighed subtraction over I_{EP} ($I = I_{EP} - \gamma_c * I_{BP}$) the main features of the ZnO PL are obtained without the influence of the GaN substrate.

The below gap PL of ZnO samples 1 and 3 is shown in Figure 9. For sample 1 (black curve) there is a broad band emission centered in ~ 517 nm (~ 2.40 eV). Also, sample 3 (red curve) exhibits a very intense PL (relativity to the sample 1 PL) centered in ~ 569 nm (~ 2.18 eV).

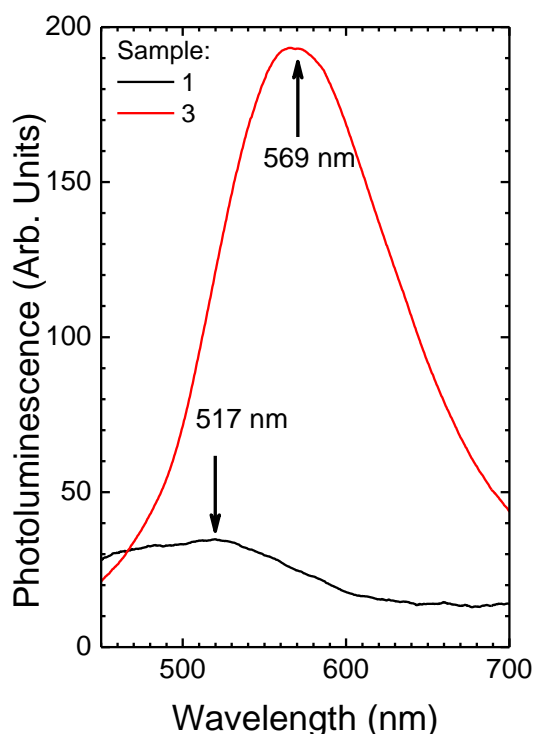


Figure 9. PL spectra of samples 1 (black line) and 3 (red line).

Although the shift of the peak from sample 3 to sample 1 is in the expected direction, if it is attributed to strain effects, the shift is too large and the values do not agree with previous reports [36]. Therefore the origin of the PL for each sample may be different. The first one (sample 1) is in good agreement with the well-known ZnO green band [29] while the second one (sample 3, peaked at the

yellow) may have a contribution of either green or orange-red bands [29, 37, 38], as its spectrum is very wide (~ 150 nm). The origin of these bands has been widely studied and is still controversial [37, 38] but the more accepted interpretation is based on an energy diagram for the different intrinsic defects that has been originally proposed from theoretical calculations [39] and improved by comparison with experimental results [40]. Within this picture both band can be originated in transitions between conduction band to deep states or donor to deep states. It is well accepted that the donor state is interstitial Zn (Zn_i). For the ZnO green band centered at ~ 500 nm it is usually reported that the deep states could be originated by O vacancies (V_O). For the ZnO orange-red band, commonly located at ~ 600 nm, the deep states could be attributed to interstitial O (O_i).

The higher PL of sample 3 may be in principle due to its larger thickness (see Table 1), however the ratio between the peaks intensities is ~ 6.3, i. e. larger than the ratio between the thicknesses ~ 3.4. Moreover the spectra drastically change. Under the previous picture of PL origin it must be concluded that sample 3 has a larger density of intrinsic defects, such as Zn_i , V_O and O_i than sample 1. This larger density may be originated in the strain relaxation previously reported, as this relaxations lead to the existence of Zn and O atoms in non-equilibrium positions.

4. CONCLUSIONS

The XRD structural study shows the epitaxial growth of ZnO films deposited on GaN substrate by an electrochemical technique employing a non aqueous solvent (DMSO). Specifically, the *c* axis is perpendicular to the plane of the substrate, while *a* and *b* axes are aligned with the respective lattice parameters of the substrate. Due to the similarity of both crystal structures, and the close values of their lattice parameters, it is hard to discriminate between substrate and film reflections, both in the reciprocal and real space. However, for thinner films we detected a component under in-plane compression while thicker films presumably relax. For sample-1, the obtained Poisson's ratio for ZnO is in good agreement with tabulated values, indicating a real effect of elastic deformation and confirming the consistency of our analysis.

The study of the optical properties of ZnO film is complicated by the similarity between the optical properties of ZnO and GaN present in the substrate. However, although the transmittance spectra have a very similar general shape in comparison with the one of the substrate, there is an increase in the total optical transmittance due to the presence of ZnO. This can be ascribed to an antireflective effect originated by the intermediate index of refraction of ZnO, and is also observed in the diffused reflectance which decreases due to transmittance increase (in the visible region). Moreover the diffused reflectance spectra show an increased absorption close to 400 nm in comparison with the substrate, which is due to ZnO. The PL between stressed and relaxed samples also changes drastically, which can be originated in a different density of defects in the samples.

ACKNOWLEDGEMENTS.

This work was supported by FONDECYT (Chile) project 1080195 and DII, PUCV, project 366 037.108/2008. This work was partially supported by CSIC (Comisión Sectorial de Investigación

Científica) of the Universidad de la República, in Montevideo, Uruguay, PEDECIBA – Física and ANII (Agencia Nacional de Investigación e Innovación).

References

1. T. Yamamoto, T. Shiosaki, and A. Kawabata, *J. Appl. Phys.* 51 (1980) 3113.
2. T. Mitsuyu, S. Ono, and K. Wasa, *J. Appl. Phys.* 51 (1980) 2464.
3. A. Hachigo, H. Nakahata, K. Higaki, S. Fujii, and S. Shikata, *Appl. Phys. Lett.* 65 (1994) 2556.
4. J.N. Dai, H.C. Liu, W.Q. Fang, L. Wang, Y. Pu, Y.F. Chen and F.Y. Jiang, *J. Cryst. Growth* 283 (2005) 93.
5. J.M. Pierce, B.T. Adekore, R.F. Davis and F.A. Stevie, *J. Cryst. Growth* 277 (2005) 345.
6. M. Kumar, R.M. Mehra, A. Wakahara, M. Ishida and A. Yoshida, *Thin Solid Films* 484 (2005) 174.
7. D.C. Oh, A. Setiawan, J.J. Kim, H. Ko, H. Makino, T. Hanada, M.W. Cho and T. Yao, *Curr. Appl. Phys.* 4 (2001) 625.
8. Y. Xiaoli, C. Nuof, Y. Zhigang, Z. Xingwang, L. Yang, Y. Jingbi, W. Yu, D. Jingjing, C. Min, G. Yun, H. Tianma, C. Xiaofeng and W. Yanshuo, *J. Semicond.* 3, (2010) 093001.
9. D. Andeen, J.H. Kim, F.F. Lange, G.K.L. Goh and S. Tripathy, *Adv. Funct. Mater.* 16 (2206) 799.
10. J.H. Kim, E.M. Kim, D. Andeen, D. Thompson, S.P. DenBaars and F.F. Lange, *Adv. Funct. Mater.* 17 (2007) 463.
11. T. Pauporté and D. Lincot, *Appl. Phys. Lett.* 75 (2009) 3817.
12. T. Pauporté, R. Cortés, M. Froment, B. Beaumont and D. Lincot, *Chem. Mater.* 14 (2002) 4702.
13. T. Pauporté, T. Yoshida, R. Cortés, M. Froment and D. Lincot, *J. Phys. Chem. B* 107 (2003) 10077.
14. T. Pauporté, D. Lincot, B. Viana and F. Pellé, *Appl. Phys. Lett.* 89 (2006) 233112.
15. O. Lupan, T. Pauporté, B. Viana, M. Tiginyanu, V. V. Ursaki and R. Cortés, *Appl. Mater. Interfaces* 2 (2010) 2085.
16. D. Lincot, *MRS Bulletin* 35 (2010) 778.
17. D. Gal, G. Hodes, D. Lincot and H.W. Schock, *Thin Solid Films* 361 (2000) 79.
18. R. Henríquez, H. Gomez, P. Grez, D. Lincot, M. Froment, E. A. Dalchiele and G. Riveros, *Electrochem. Solid-State Lett.* 10 (2007) D134.
19. H. Gómez, G. Riveros, D. Ramirez, R. Henríquez, R. Schrebler, R. Marotti and E. A. Dalchiele, *J. Solid State Electrochem.* 16 (2012) 197.
20. Y. Liua and J. Zhang, *Scr. Mater.* 63 (2010) 109.
21. J. Elias, R. Tena-Zaera, and C. Lévy-Clément, *J. Electroanal. Chem.* 621 (2008) 171.
22. S.R. Johnson and T. Tiedje, *J. Appl. Phys.* 78 (1995) 5609.
23. J.L. Pankove, *Optical Processes in Semiconductors*, Dover Publications, New York (1971).
24. S. Y. Kim, Y. S. Yeon, S. M. Park, J. H. Kim and J. K. Song, *Chem. Phys. Lett.* 462 (2008) 100.
25. H. Caia, H. Shen, Y. Yin, L. Lu, J. Shen and Z. Tang, *J. Phys. Chem. Solids* 70 (2009) 967.
26. L. L. Yang, Q. X. Zhao, M. Willander, J. H. Yang and I. Ivanov, *J. Appl. Phys.* 105 (2009) 053503.
27. S. Chawla, N. Karar and H. Chander, *Physica B* 405 (2010) 198.
28. R. Bhargava In: R. Bhargava (Ed.), *Properties of Wide Bandgap II–VI Semiconductors*, EMIS Datareviews Series No. 17, London (1997)
29. Ü. Özgür, Y. I. Alivov, C. Liu, A. Teke, M. A. Reshchikov, S. Doğan, V. Avrutin, S.-J. Cho and H. Morkoc, *J. Appl. Phys.* 98 (2005) 041301.
30. D. P. Norton., Y. W. Heo, M. P. Ivill, K. Ip, S. J. Pearton, M. F. Chisholm and T. Steiner, *Mater. Today* 7 (2004) 34.
31. K. Keis and A. Roos, *Opt. Mater.* 20 (2002) 35.

32. R. E. Marotti, D. N. Guerra, C. Bello, G. Machado and E. A. Dalchiele, *Sol. Energy Mater. Sol. Cells* 82 (2004) 85.
33. C. D. Bojorge, H. R. Cánepa, U. E. Gilabert, D. Silva, E. A. Dalchiele and R. E. Marotti, *J. Mater. Sci.: Mater. Electron.* 18 (2007) 1119.
34. C. D. Bojorge, V. R. Kent, E. Teliz, H. R. Cánepa, R. Henríquez, H. Gómez, R. E. Marotti and E. A. Dalchiele, *Phys. Stat. Sol. A* 208 (2011) 1662.
35. W. Shan, T. J. Schmidt, R. J. Hauenstein, J. J. Song and B. Goldenberg, *Appl. Phys. Lett.* 66 (1995) 3492.
36. W. Shan, W. Walukiewicz, J. W. Ager III, K. M. Yu, Y. Zhang, S. S. Mao, R. Kling, C. Kirchner and A. Waag, *Appl. Phys. Lett.* 86 (2005) 153117.
37. A. B. Djuricic, Y. H. Leung, K. H. Tam, L. Ding, W. K. Ge, H. Y. Chen and S. Gwo, *Appl. Phys. Lett.* 88 (2006) 103107.
38. H. S. Kang, J. W. Kim, S. H. Lim, H. W. Chang, G. H. Kim, J. H. Kim and S. Y. Lee, *Superlattice Microst.* 39 (2006) 193.
39. B. Lin, Z. Fu and Y. Jia, *Appl. Phys. Lett.* 79 (2001) 943.
40. C. H. Ahn, Y. Y. Kim, D. C. Kim, S. K. Mohanta and H. K. Cho, *J. Appl. Phys.* 105 (2009) 013502.